Article

Nature-Inspired Superhydrophobic Sand Mulches Increase Agricultural Productivity and Water-Use Efficiency in Arid Regions

Adair Gallo, Jr., Kennedy Odokonyero, Magdi A. A. Mousa, Joel Reihmer, Samir Al-Mashharawi, Ramona Marasco, Edelberto Manalastas, Mitchell J. L. Morton, Daniele Daffonchio, Matthew F. McCabe, Mark Tester, and Himanshu Mishra*

Read Online

ACCESS | 📊 Metrics & More | 📰 Article Recommendations | 🆂🅸 Supporting Information

ABSTRACT: Excessive evaporative loss of water from the topsoil in arid-land agriculture is compensated via irrigation that exploits massive freshwater resources. The cumulative effects of decades of unsustainable freshwater withdrawals in many arid regions are now threatening food−water security. While plastic mulches can reduce evaporation from the topsoil, their cost and nonbiodegradability limit their utility. In response, we report on biodegradable superhydrophobic sand (SHS), a bioinspired enhancement of common sand with a nanoscale wax coating. When SHS was applied as a 5−10 mm-thick mulch over the soil, evaporation was reduced by 56−78% and soil moisture increased by 25−45%, which benefited the development of crops. Multiyear field trials with tomato (*Solanum lycopersicum*), barley (*Hordeum vulgare*), and wheat (*Triticum aestivum*) under normal irrigation demonstrated that SHS mulch application enhanced yields by 17−73%. Under brackish water irrigation (5500 ppm NaCl), SHS mulching produced 53−208% higher fruit and grain yields for tomato and barley crops, respectively. SHS application did not affect the soil−root−rhizosphere microbial communities as evidenced by 16S rRNA gene analysis. The rhizospheric environments were dominated by an assemblage of diverse bacterial communities, such as *Gammaproteobacteria*, *Alphaproteobacteria*, and *Bacteroidetes*, followed by *Firmicutes*, *Gemmatimonadetes*, and *Actinobacteria*, which could be responsible for the degradation of paraffin wax on the SHS. Thus, SHS technology should benefit irrigated agriculture and city-greening efforts in arid regions under the constraint of high water-use efficiency.

KEYWORDS: food−water security, superhydrophobic sand, water-use efficiency, bioinspiration, mulching, sustainability

■ INTRODUCTION

The importance of irrigation toward humanity's ability to produce food cannot be overstated. For example, while only 20% of cultivated land is irrigated, this fraction contributes 33−40% of the total world food production.[1,2] Unfortunately, this outsized contribution to food production comes at a price, consuming over 70% of global freshwater withdrawals annually.[2−5] Regions with arid and semi-arid climates, such as the Middle East, northern Africa, the northwest Indian subcontinent, and western Australia, rely on limited freshwater resources to grow food for sustenance and trade.[3] The plants growing in these regions depend on the soil moisture content for nutrient uptake, optimal temperature regulation, and salt stress reduction.[6] However, due to intense solar radiation and direct exposure to dry air and winds, a significant fraction of the water supplied to soils is lost to evaporation.[7] Therefore, to ensure sufficient water availability to support plant growth, excessive volumes of ground and surface waters are routinely withdrawn; this has critically depleted water supplies in many parts of the world,[8] resulting in food and water security concerns as issues of international importance.[9−14]

Technologies for enhancing the water-use efficiency of irrigated agriculture, i.e., growing more food/biomass with less water, are warranted for a sustainable future. Subsurface impermeable layers are sometimes employed to limit water loss due to percolation; however, their installation is expensive and labor-intensive.[15−17] As an alternative, the soil surface can be covered with plastic mulches to reduce evaporation, enhance crop yield, and to reduce the incidence of pests and weeds and nutrient leaching.[6,18] In spite of the beneficial effects of plastic mulches,[19−21] the approach is infrastructure-intensive and plastic landfilling is unsustainable.[18] Although biodegradable plastics are being vigorously pursued, their success has been limited to date due to their high cost, slow or incomplete biodegradability, and time-varying wetting properties after deployment.[18,22,23] In addition, there have been growing concerns about the leaching of phthalates from plastic mulches into soils and their adverse effects on the soil quality and microbial activity over the long term.[24,25]

Recently, engineered nanomaterials (ENMs) have been demonstrated to enhance the water-use efficiency of soils.[26] For example, a pot-scale study revealed that an ENM comprising electron beam-dispersed attapulgite and sodium polyacrylate polyacrylamide reduced water and nutrient loss
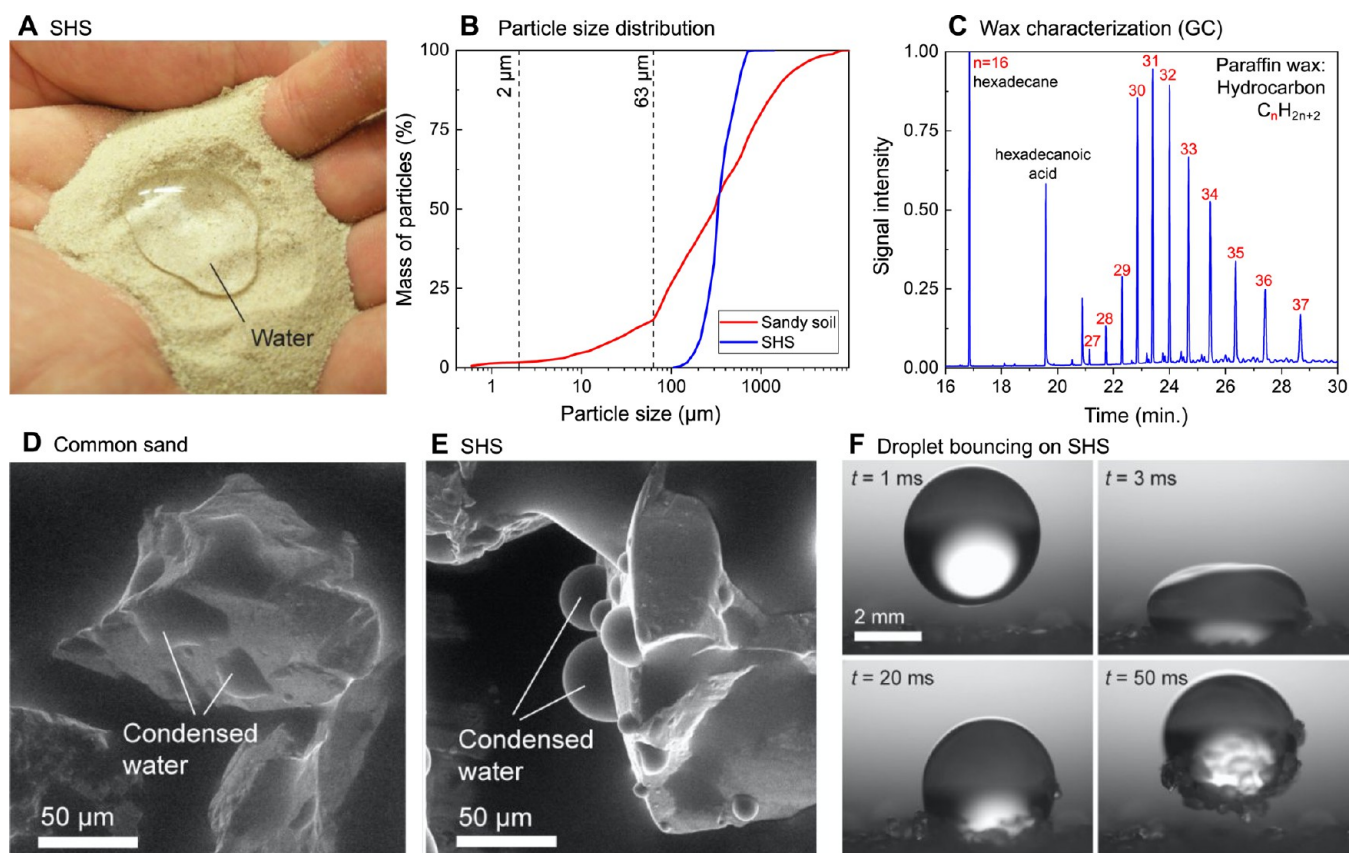
Figure 1. Characterization of superhydrophobic sand (SHS). (A) Photograph of SHS with water on top, demonstrating its superhydrophobicity. (B) Particle size distribution of SHS and sandy soil (loamy sand as per USDA soil texture characterization) collected at a local agriculture research facility. The fractions above and below 63 μm were determined using sieving and hydrometer methods,[33] respectively. (C) Gas chromatography of paraffin wax (∼0.1 M in cyclohexane) pinpointing the chain lengths of the constituent alkanes (n) in red. The relative compositions of the alkanes are presented in Table S1. Note: hexadecane and hexadecanoic acid were used as internal standards. Representative environmental scanning electron micrographs of water droplets condensed on (D) common sand grains and (E) SHS grains. The apparent contact angles of water droplets are significantly higher in (E) than in (D). (F) High-speed images of a 30 μL water droplet dropped onto a 5 mm-thick SHS layer from a height of 2 cm (Movie S1).

and boosted plant growth.[27] Although crops exposed to ENMs exhibit adaptive processes in response to environmental stresses, agronomic traits of such crops (e.g., photosynthesis, fruit yields, nutritional quality, and nitrogen fixation) may be compromised during the adaption response.[28] Despite the multiscale transdisciplinary efforts being undertaken to pinpoint their effects on soils and the microbiome,[26,29] the use of ENMs still has unknown implications for food safety and quality, in terms of underlying phytotoxicity and bioavailability.[28]

Based on the aforementioned challenges associated with the current technologies, our focus is on the development of sustainable soil mulching technology capable of reducing soil evaporation under arid land conditions. Therefore, the main objective of the present study is to develop superhydrophobic sand (SHS) mulches and evaluate their roles in increasing agricultural productivity and water-use efficiency in arid-land agriculture. As a result, we developed an innovative approach to control evaporation from soils by combining (i) common sand, a material readily available in soils of arid regions, and (ii) paraffin wax, a low-cost and biodegradable hydrophobic material that is available at an industrial scale.[30−32] Our results demonstrate that superhydrophobic sand (SHS) mulching reduces water evaporation from moist soils and that the

enhanced soil moisture promotes plant health and yield under arid conditions.

■ MATERIALS AND METHODS

Synthesis of SHS.

1. Materials:
   a. Common sand (characteristic size in the range of 100−700 μm; Figure 1B).
   b. Blocks of paraffin wax (molecular weight, 487 Da, melting point 60−65°C, C_nH_{2n+2}, where, n = 27−37, Figure 1C) grated to shavings of <1 mm size.
2. Wax shavings were dissolved in approximately 10 L of hexane.
3. Then, 50 kg of common sand was added to a 60 L evaporator (Figure S1).
4. The wax/hexane mixture was added to the evaporator flask to achieve a wax-to-sand ratio of 1:600. Note that concentrations as low as 1:2000 (wax/sand) achieved superhydrophobicity.
5. Next, the temperature of the evaporator was gradually increased from 22 to 55 °C, and the pressure was reduced from 1 atm to 100 mbar to evaporate the hexane, which was condensed and collected for reuse (recovery rate of ∼99%).
6. The pressure was normalized and SHS was collected and stored for use.

Note: Due to the flammability of the organic solvents used in this manufacturing protocol, potential sources of electrical sparks, such as cell phones, match sticks, and static charge, must be avoided and the

setup must be installed in a well-ventilated area. All components of the setup were electrically grounded to avoid any electric spark.

SHS and Paraffin Characterization. The wax used was characterized via gas chromatography−mass spectroscopy (Agilent 7890A−5975C) ($\sim 10^{-1}$ M in cyclohexane). Wetting of individual SHS particles with water was studied under an environmental scanning electron micrograph (FEI Quanta 600). Contact angles on a 10 mm bed of SHS were measured by placing a 10 μL water droplet with advancing and receding rates of 0.2 μL/s (Kruss Drop Shape Analyzer DSA100, Advance software). The thickness of the wax layer on the sand granules was estimated from the surface area of sand grains and the volume of wax used. The surface area of the sand was estimated using the Brunauer−Emmet−Teller (BET) method using krypton gas.[34]

Quantification of Evaporation Flux. Pots containing 75 g of Metro Mix 360 soil and 132 g of water were covered with either SHS mulch (0-, 5-, 10-, 15-, and 20-mm thick) or common (uncoated) sand (0-, 5-, 10-, 15-, and 20-mm thick) or were not subjected to any mulching (unmulched) and placed outside the lab under environmental conditions. All pots were in duplicate. The masses of individual pots were tracked over time with a mass balance. The experiment was started on October 10, 2016 at 9:45 a.m. at Thuwal, Saudi Arabia (22.3084° N, 39.1030° E). The environmental data were obtained from the KAUST weather station.

Quantification of Soil Moisture. We buried 30 L plastic buckets with a diameter of 35 cm at the ground level and filled them up with local sandy soil, which was sieved to remove gravel of size >1 cm. We compared the 5 mm-thick SHS mulch with the unmulched control. Bottom-perforated buckets were used to circumvent the issue of lateral percolation and to measure vertical flows, i.e., evaporation and percolation. To quantify soil moisture and temperature, we used hydraprobe sensors (Stevens Water, LLC), which exploit the principle of coaxial impedance dielectric reflectometry.[35,36] Briefly, we compared mulched and unmulched soil under two irrigation regimes: (i) single irrigation starting with supersaturated soil with no further irrigation and (ii) daily subsurface drip irrigation (1.1 L/day). The data for case (i) were determined as the average measurement of two sensors buried at a depth of 5 cm. The data for case (ii) were estimated as the average measurement of three sensors at depths of 15, 20, and 25 cm. The experiments were performed from January to April (2018) at the same site as that of our field trials (21.79° N, 39.72° E). The weather conditions of the site are presented in Figure S4.

Field Trials and Experimental Designs with Tomato, Barley, and Wheat Crops. Field trials were conducted at the agricultural research station of King Abdulaziz University, Hada Al Sham, Saudi Arabia (21.7963° N, 39.7265° E) using the tomato (*S. lycopersicum*) varieties A (Bushra) and B (Nunhem's Tristar F1), wheat (*T. aestivum*) variety Balady, and barley (*H. vulgare*) variety Morex. The field was divided into plots of 2.5 × 2.5 m for each treatment, with plants uniformly spaced within each plot. A replicated split plot design was used with the same treatments designated to the same individual plots. The total number of tomato plants per plot was 12 and 15 in the years 2018 and 2019, respectively. For barley and wheat, the seeds were spread in a line 2.5 m long and 5 cm deep, with 15 cm line spacing in between. The distance between the plants was adjusted at approximately 2 cm by thinning them after full germination. To control the thickness of the SHS mulch, we used a cardboard template of known area and homogeneously applied a specific mass of SHS (Movie S2). Tomato fields received SHS mulch as a 40 cm strip around the plants in a line for the 2018 season and as 40 cm-diameter circles around each plant for the 2019 season to save on materials. On the other hand, barley and wheat fields were completely covered with the SHS mulch due to the close proximity between plants. Plastic mulches (120 μm-thick polyethylene sheets) were also applied over the whole plot. For the subsurface drip irrigation system, we used a Rain Bird LD-06-12-1000 Landscape drip, 0.9 gallon/h (3.4 L/h per dripping point). The plants were fertilized through the irrigation system using common compound fertilizers on a weekly basis (N/P/K 20:20:20 during the vegetative stage and N/P/K 10:10:40 at the

flowering and fruiting stages). For the 2019 season, there were two plots with 5 mm-thick SHS mulch, clear plastic (transparent 120 μm-thick polyethylene sheet), and black plastic (120 μm-thick polyethylene sheet) and four plots with 10 mm-thick SHS and unmulched controls. The number of plants in replicated plots varied according to the treatment, as evidenced by the number of dots in Figure 5A,B; hence, the experiments involved an incomplete split plot structure. More details are presented in Section II of the Supporting Information (Figures S4−S10).

At harvest time, tomato fruits were harvested weekly and collected in plastic bags labeled with the plant identity number, followed by counting and weighing. Harvests were conducted for 6 weeks, and the total number and mass of fruits per plant were considered for data analysis. Barley and wheat plants were collected at the end of the growing season, and the number of plants was counted over a homogeneous area of 1 m^2 inside each plot. The plants were manually separated and counted, followed by extrapolating the yield per plant to yield per m^2 by multiplying the total number of plants in the measured area by the mass of grains per plant (Figure 5B). Extrapolation to m^2 was preferred to avoid the inherent difficulty in separating one plant from another due to their close proximity and tangled roots. Statistical analysis of the treatments was performed in Matlab R2019b using the Kruskal−Wallis H test, where (*S*) in Figure 5 represents statistical significance ($p < 0.05$). In addition, we performed soil analysis for all plots to guarantee homogeneity within the field; the details are presented in Section III of the Supporting Information.

Analysis of Soil−Root Microbiomes. Soil samples were collected during the 2018 crop season (20th February 2018) from our field trial site (21.79° N, 39.72° E). For each field treatment (irrigation: fresh/brackish water and overlay: SHS mulches presence/absence), the root systems of barley and tomato plants were randomly selected from each experimental plot (barley, *n* = 18; tomato, *n* = 18; Table S5). After gently removing the plants from the soil, the root system was sampled using a pair of sterile scissors and tweezers. The rhizosphere was separated from the root tissues, as described previously.[37] The obtained root tissues were surface-sterilized according to a previously reported methodology.[38] All samples were stored at −20 °C for molecular analysis. Bulk soil samples were also collected from the unvegetated area of each experimental plot (0.5−10 cm depth; 18 soil samples, *n* = 18, for each of the two crops).

DNA was extracted from 0.5 ± 0.05 g of bulk and rhizosphere soils using a PowerSoil DNA isolation kit (MoBio Inc.). Surface-sterilized root tissues were ground in a mortar and pestle using liquid nitrogen, followed by DNA extraction from 1 gram of the ground root tissues using a DNeasy Plant Maxi kit (Qiagen, Germany). The V3−V4 hypervariable regions of the 16S rRNA gene were PCR-amplified using the universal primers 341F and 785R.[39] Libraries were constructed using a 96 Nextera XT Index Kit (Illumina) following the manufacturer's instructions and sequenced using the Illumina MiSeq platform at the Bioscience Core Lab at KAUST. Raw sequences were analyzed using the DADA2 pipeline, including quality filtering, trimming, dereplication, and paired-end merging of the sequences.[40] Chloroplast- and mitochondria-classified sequence variants (SVs) were discarded, and non-prevalent SVs (defined as SV present in <1% of our samples) were removed from the SV table. A total of 13 568 983 sequences (barley: 8 611 818 and tomato: 4 194 505) divided into 6912 SVs were obtained. Only samples with suitable sequencing depth and diversity (Good's coverage value > 99%) were used for further analysis. The raw reads have been deposited in the Short Read Archive of the NCBI under the accession numbers SUB7136748, SUB7211346, and SUB7137862.

The β-diversity of the bacterial communities in barley and tomato was analyzed using the compositional similarity matrices (Bray−Curtis) of the relative log-transformed SV tables using a previously reported methodology.[41] The same matrices were also used to perform unconstrained analysis of principal coordinates and to assess the compositional variation explained by each experimental factor. Permutational multivariate analyses of variance (PERMANOVA) were performed using the *Adonis* function from the "vegan" package[42]
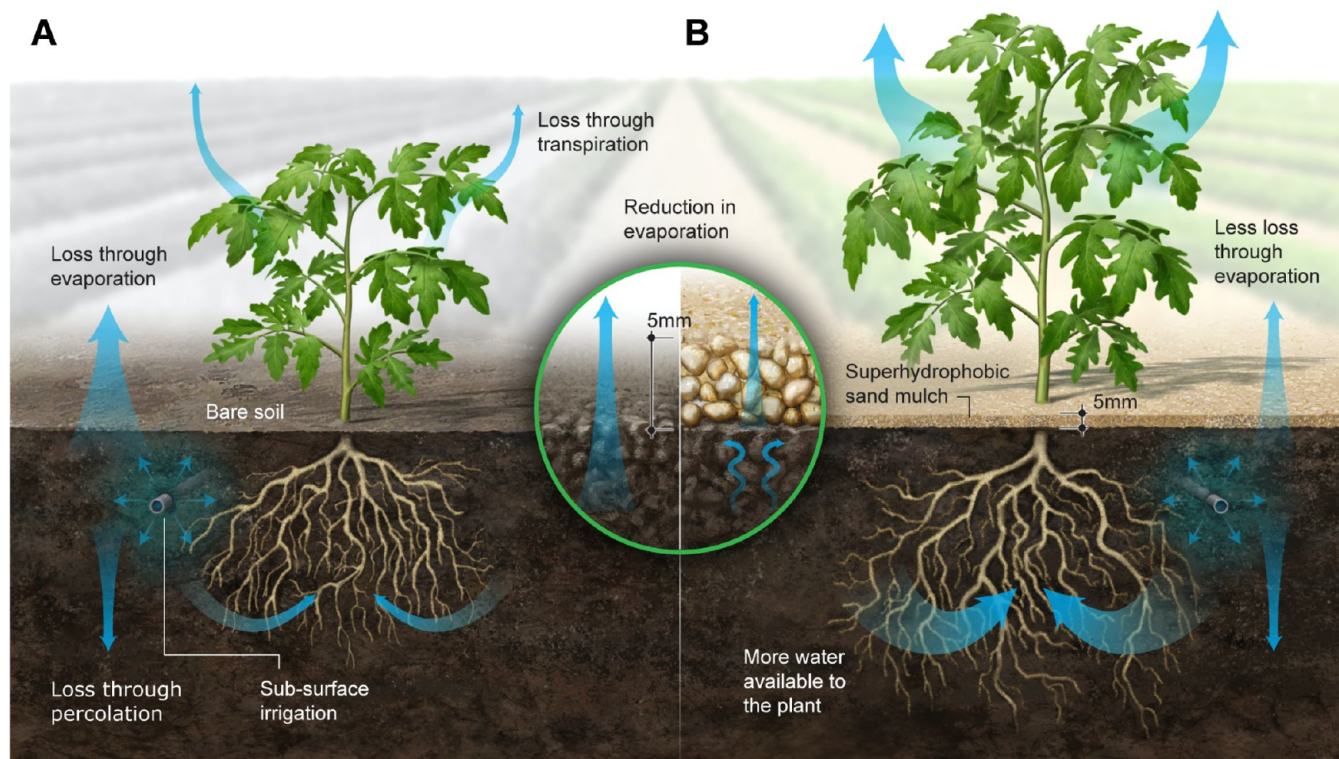
Figure 2. Concept of superhydrophobic sand (SHS) mulches to reduce water evaporation from soils in arid regions. Water movements for subsurface-irrigated (A) unmulched soil and (B) soil mulched with SHS. SHS prevents the capillary rise of water, thereby creating a dry diffusion barrier that allows water vapor to diffuse at a rate significantly lower than that in unmulched or bare soil.

to statistically test the impact of each experimental factor: "irrigation" (two levels: fresh and brackish water), "overlay" (two levels: SHS mulch and unmulched soil), and "compartment" (three levels: root tissues, rhizosphere, and bulk soil). Furthermore, PERMANOVA pairwise tests were conducted to evaluate the effect of overlay on each interaction category compartment × irrigation using PRIMER.[41]

RESULTS

Physicochemical Properties. In nature, several super-water-repellent plants and animals exploit waxy cocktails and micro- or nanotextures to achieve extreme water repellence, also known as superhydrophobicity, to perform critical functions, including fog harvesting under arid conditions,[43] skating on and launching from the water surface to avoid predators,[44,45] directing the movement of condensed water,[46,47] and respiring under water.[48] Analogously, SHS comprises common sand grains coated with a nanoscale layer of paraffin wax (Figure 1A). SHS was produced by dissolving common paraffin wax in hexane, mixing the solution with common sand, and evaporating hexane from the mixture at ∼100 mbar and 55°C (Figure S1). Then, hexane was simultaneously condensed and collected in a separate container for reuse during the process. The sand comprised silica particles 100−700 μm in diameter (Figure 1B). Paraffin wax was a mixture of hydrocarbons with 27−37 carbons in length (Figures 1C, S2, and Table S1). This process led to the formation of a ∼20 nm-thick wax coating onto the sand grains, which we estimated from the volume of the wax to the sand surface area. Using BET analysis, we determined the surface area of our sand to be ∼0.11 m^2/g. For 1 g of wax of mass density 800 kg/m^3, the volume was 1.25×10^{-6} m^3, whereas for 600 g of sand, the surface area was 600 g × 0.11 m^2/g = 66 m^2. Assuming uniform coating, the average thickness of the

wax layer was 1.25×10^{-6} m^3/66 m^2 = 1.8×10^{-8} m ≈ 20 nm. In addition to hexane, pentane, octane, cyclohexane, diethyl ether, dichloromethane, methyl-*tert*-butyl ether, petroleum ether (ligroin), chloroform, tetrahydrofuran, and triethyl amine were tested as solvents; however, no significant differences were observed with respect to their water-repellent properties. Furthermore, a variety of natural waxes were also tested, including palm wax, soy wax, and beeswax; the resultant sand exhibited the same superhydrophobicity. Given the scale of agricultural operations, we chose to use paraffin wax. In more recent developments, we have observed that the solvent can be completely eliminated and replaced by vigorous mixing at 70−80 °C for approximately 30 min without noticeably compromising the coating. The complete elimination of the solvent might be a crucial step toward scalability of this technology.

The water repellency of sand grains dramatically increased after the above-described surface enhancement (Figure 1A). The grain-level apparent contact angles, θ_r, of water micro-droplets formed by condensing water vapor on individual sand grains increased from $\theta_r \approx 30°$ (for ordinary sand) to $\theta_r \approx 105°$ for SHS (Figure 1D−E). The advancing (θ_A) and receding (θ_R) contact angles of ≈10 μL of water droplets advanced and retracted at 0.2 μL/s on ∼10 mm-thick SHS layers were $\theta_A \approx 160°$ and $\theta_R \approx 150°$, respectively, which are the characteristics of superhydrophobicity (Materials and Methods section). Water droplets of ∼30 μL impacted a 5 mm-thick layer of SHS from a height of ∼2 cm and bounced off and relanded, forming liquid marbles[49,50] (Figure 1F). The factors and mechanisms underlying the superhydrophobicity of SHS are presented in the Discussion section. Next, we characterized the breakthrough pressure of water on SHS,
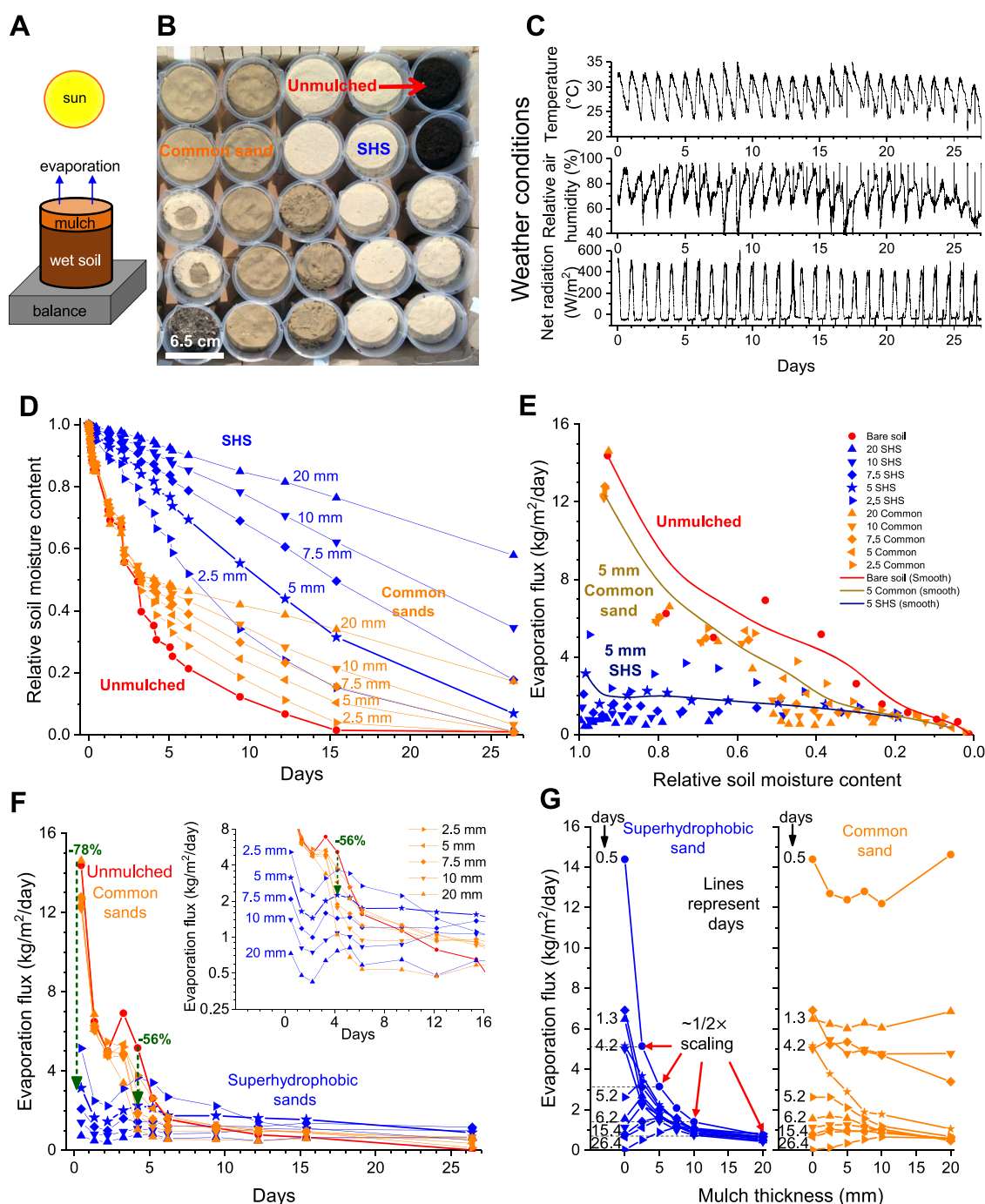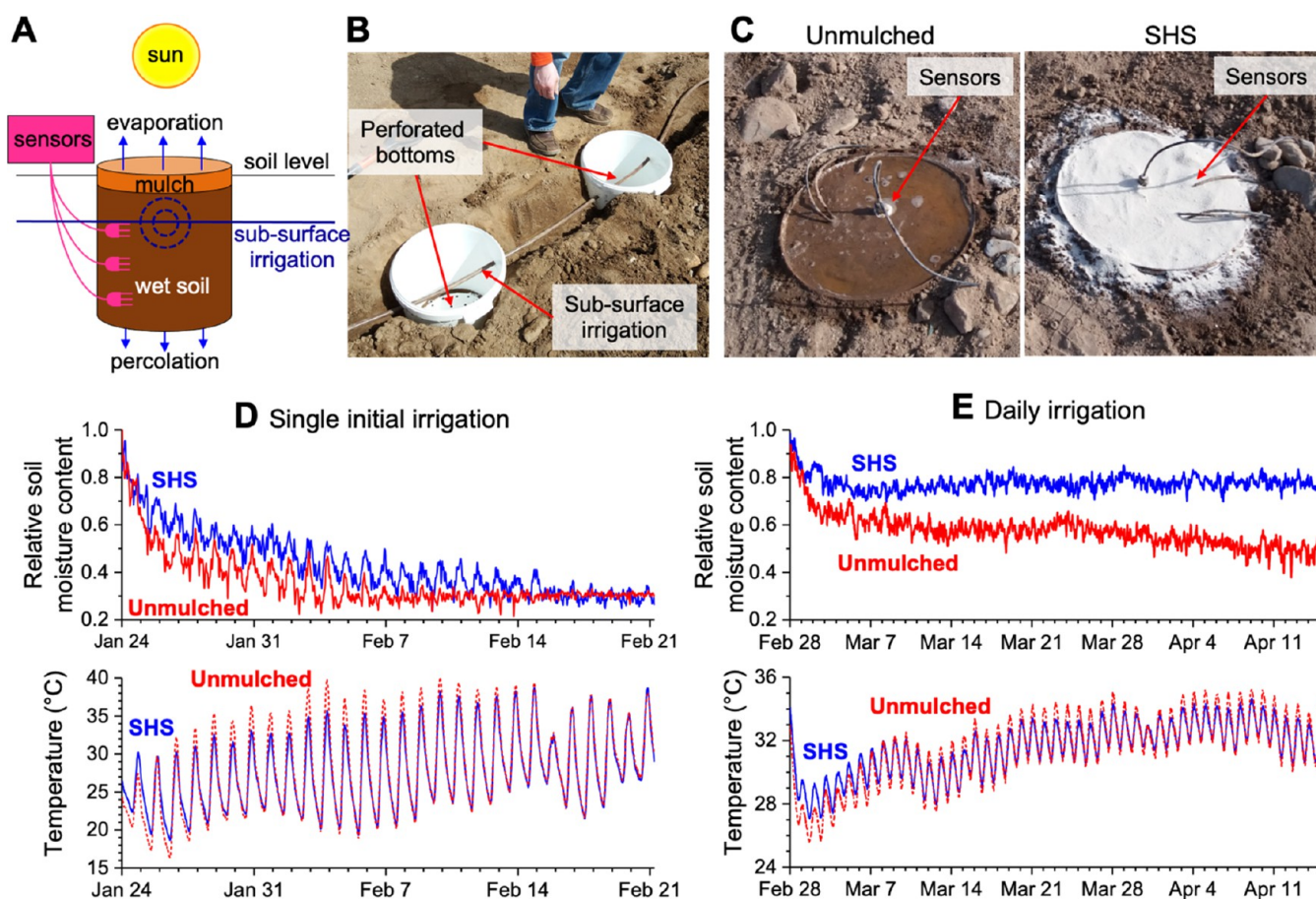
Figure 3. Effects of superhydrophobic sand (SHS) mulching on water loss via evaporation from soil. We gravimetrically measured water loss from (bottom-closed) pots containing initially wet soil under various thicknesses of common sand and SHS mulches (0−20 mm, indicated by the number preceding the unit "mm") exposed to environmental conditions. SHS mulch reduced evaporation from the topsoil in proportion to its thickness. (A) Schematic of the experimental setup showing evaporation loss from a single pot. (B) Photograph of the pots on the first day revealing mulches with dark-colored common sand as they absorbed water from the soil underneath, whereas SHS stayed dry. (C) Weather conditions during the period of the experiment. (D) Relative water loss from soil under different mulching conditions. (E) Evaporation flux as a function of the relative soil moisture content. (F) Evaporation flux as a function of time. (G) Evaporation flux as a function of mulch thickness (Note: each curve represents the evaporative flux on a specific day as a function of mulch thickness; zero on the abscissa represents unmulched soil). The standard error was below 7% ($\sigma_{\bar{x}} = \sigma/\sqrt{N}$, where σ is the standard deviation of the duplicates, $N = 2$).

defined as the pressure at which water penetrates into the microtexture.[51] While water spontaneously imbibes into common sand, due to capillarity,[52] a 5 mm-thick SHS layer could prevent imbibition of the water column up to a height of $h \leq 12$ cm, thereby presenting a breakthrough pressure of $P_h = \rho g h \approx 1.2$ kPa (as explained in the Discussion section). Based

on these results, we envisioned that when placed on moist topsoil, SHS would create a capillary and diffusion barrier for soil moisture and insulate it from direct exposure to solar radiation, wind, and dry air (Figure 2). The hypothesis that we tested was that adding a superhydrophobic material on top of soil would reduce evaporative losses, increase the soil moisture
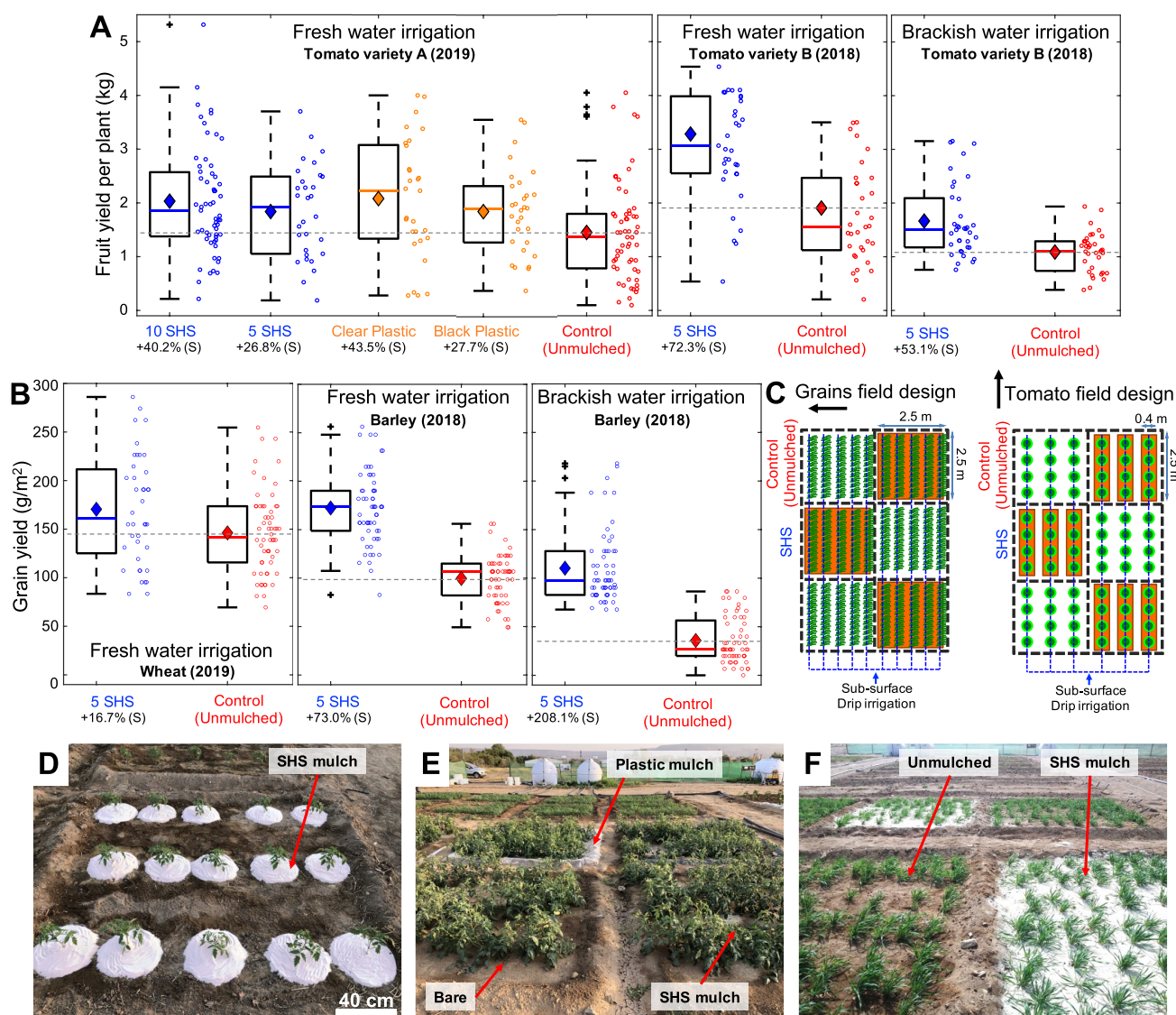
Figure 4. Effects of superhydrophobic sand (SHS) mulching on the soil moisture content. We used sensors to measure the effects of a 5 mm-thick SHS mulch layer on the soil moisture content and soil temperature exposed to field conditions. (A) Schematic of the experimental setup showing evaporation loss and soil moisture/temperature sensors in a bottom-perforated bucket buried at the soil level for a more realistic soil temperature profile. One irrigation line with a single dripping point passed through the buckets at a depth of approximately 10 cm. (B, C) Photographs of the experimental setup during installation and just after SHS application in one of the buckets. (D, E) Average soil moisture and temperature for two sets of experiments: (D) single initial irrigation event up to saturation and another with (E) one initial irrigation to saturation followed by daily irrigation. In (D), the data were collected at a depth of 5 cm. In (E), the data represent the average of soil moisture and temperature from the following depths: 15, 20, and 25 cm. The soil moisture content significantly increased after SHS mulching, particularly in the case of daily irrigation. Mulching also reduced the highest daily temperatures, except during the first few days, when evaporative cooling was very high for unmulched soil.

content, and possibly benefit crops grown in water-scarce environments.

Effects of SHS Mulching on the Evaporation Flux and Soil Moisture Content. To test our hypothesis, we evaluated the effects of SHS mulching on evaporation rates from the topsoil and soil moisture content and compared them with the effects of mulching with common sand and unmulched (control) sand. Compared to mulching with untreated sand and unmulched controls, SHS mulching dramatically decreased water loss via evaporation (Figure 3D). During the first few days, while the soil moisture was still high, the evaporation flux of the pots mulched with untreated sand was high, similar to that of the controls (Figure 3F). In contrast, the evaporation flux of SHS-mulched pots was lower and mostly independent of the soil moisture content (Figure 3E). Remarkably, a 5 mm-thick SHS mulch layer reduced the evaporation flux from approximately 78−56% during the first 4 days of the experiment (Figure 3F). Evaporation flux, J, was inversely proportional to SHS mulch thickness, L_{SHS}, such that $J \propto (L_{SHS})^{-1}$; as the mulch thickness doubled, the evaporative flux decreased by approximately 50% (Figure 3G).

Next, we quantified the effects of 5 mm-thick SHS mulches on the soil moisture content at a farm with loamy sand soil at a field station located in Hada Al-Sham, Saudi Arabia (21.79° N, 39.72° E) and compared it with those of unmulched soil (control). Unlike the pot-scale experiment, this setup facilitated percolation. We installed soil moisture and temperature sensors that were specifically calibrated for this soil in bottom-perforated buckets that prevented the lateral flow of water while maintaining a vertical flux. The buckets were then buried to the soil level to minimize unrealistic soil temperature profiles during day/night cycles (Figure 4A−C). We studied two irrigation scenarios: (i) single irrigation starting from supersaturated soil with no further water application (Figure 4D) and (ii) daily irrigation using a subsurface drip system, also started from supersaturated soil (Figure 4B,E). As both systems started from supersaturation, there were minimal differences in the beginning due to water loss via percolation in either case. However, as percolation abated, the effects of mulching on the soil moisture content became apparent: the moisture content in the top 5 cm of the unmulched soil was lost after approximately 14 days; in contrast, while it took approximately 23 days for mulched soil to dry out (Figure 4D).

Figure 5. Effects of superhydrophobic sand (SHS) mulching on the performance of tomatoes, barley, and wheat in field trials. Results for plants grown under 5−10 mm superhydrophobic sand (5−10 SHS) mulches (blue) versus unmulched soil (red) and plastic mulches (orange) on tomato (A) fresh fruit yield and (B) barley and wheat grain yield. (C) Schematics of the field designs for grains with the SHS mulch completely covering the plot and tomato with the SHS mulch as 40 cm strips or circles around the plants. Photographs showing (D, E) tomato and (F) barley fields with arrows detailing the unmulched, SHS, and plastic mulch plots. SHS mulching significantly increased the yields of tomatoes, barley, and wheat. Dots in the boxplots represent the measurements for individual plants from replicate plots. Each dot represents the total mass of fruits produced per plant for tomatoes. The mass of grains per area is presented for barley and wheat. Each treatment was compared with the control (unmulched) case using the Kruskal−Wallis H test, where (S) represents statistical significance ($p < 0.05$) and percent change is the relative difference of the means. The boxes contain the middle 50% of the data points, with the horizontal line indicating the median and the diamond inside the box indicating the mean.

Next, in the daily irrigation setup, soil moisture achieved steady states in approximately a week, such that the soil moisture of mulched soil was approximately 25−45% higher than that of unmulched soil (Figure 4E). Interestingly, the evaporation rates from unmulched supersaturated soil were quite high during the first few days, resulting in evaporative cooling, as evidenced by temperature data. These trends, however, reversed after a few days because evaporative cooling diminished at a steady state, such that the temperature of mulched soil was 1−3 °C cooler than that of unmulched soil (Figure 4D,E; bottom panels).

Effects of SHS Mulching on Crop Yields. To test whether the higher soil moisture content was substantial to

affect crop yields, we investigated the effects of SHS mulching on the production of different selected crops under real arid conditions at our field station located at Hada Al-Sham, Saudi Arabia (21.79° N, 39.72° E). We conducted multiyear field trials using a high-value crop (tomato, *S. lycopersicum*—variety A, cv. Bushra; variety B, cv. Nunhem's Tristar F1) and two large-scale grass crops (barley, *H. vulgare*, cv. Morex, and wheat, *T. aestivum*, cv. Balady) to broaden the understanding on different plants. We compared the beneficial effects of SHS mulches of 5−10 mm thickness with those of 120 μm-thick polyethylene sheets (hereafter referred to as plastic mulches) and unmulched soil (control). Two types of irrigation scenarios were investigated: (i) normal freshwater irrigation
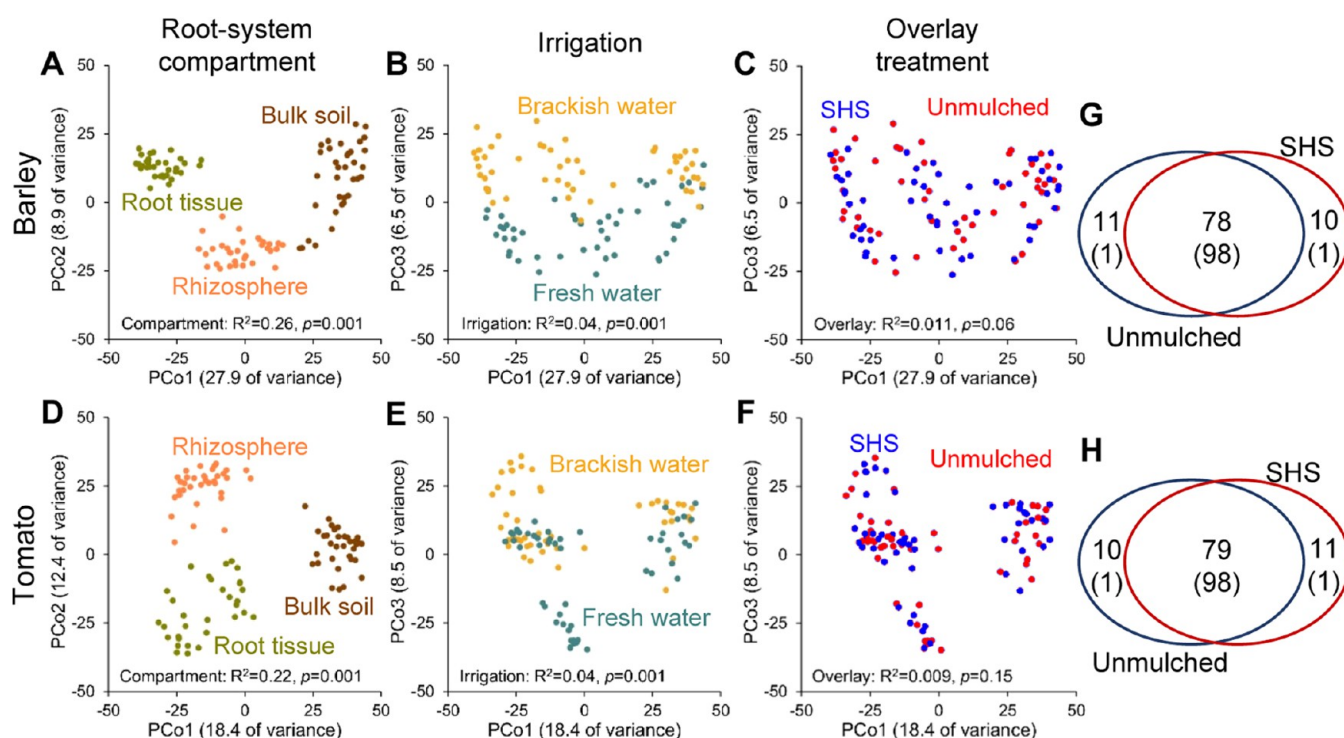
Figure 6. Unconstrained analysis of principal coordinates conducted on the root system-associated bacterial communities. We used the tested experimental factors (compartmentalization, irrigation type, and overlay treatment) to evaluate the variations in the overall composition of the bacterial communities in (A–C) barley and (D–F) tomato. The Venn diagram shows the percentages of bacterial sequence variants (SV) shared among overlay treatments (unmulched soil and SHS mulch) in the root system (root and rhizosphere) and bulk soil of (G) barley and (H) tomato. SV percentages are indicated by large areas, whereas the relative abundances of SVs are reported in parenthesis.

(<900 ppm NaCl) applied twice a day through subsurface drip irrigation and (ii) brackish irrigation (5000 ppm NaCl) applied twice a day (Figure 5). Due to harsh weather conditions during summer seasons, the crops were sown during the November–December period (winter 2017 and 2018) and were subsequently harvested during March–April of the following years (Figures S4–S10).

Compared with unmulched controls, SHS mulching led to significant improvements in tomato yields under both normal and brackish water irrigation (Figure 5A). The most significant result was obtained for the 5 mm-thick SHS mulch under normal irrigation for tomato, variety B (2018 season), which achieved a 72% improvement in yield relative to that obtained for unmulched controls. The yield enhancements for variety A with 5 and 10 mm-thick SHS mulches under normal irrigation were 27 and 40%, respectively, compared with those for unmulched controls. In fact, the performance of SHS mulching was on par with plastic mulches for tomato variety A, where black and clear plastic mulches enhanced crop yields by 28 and 43%, respectively. In our experiments with brackish water irrigation, the 5 mm-thick SHS mulch enhanced the yield of tomato variety B by 53% compared with that of unmulched controls (Figure 5A). All of these results were statistically significant at $p < 0.05$ (Kruskal–Wallis H test).

We also observed statistically significant enhancements in the yield of barley mulched with the 5 mm-thick SHS mulch under normal (73%) and brackish water (208%) irrigation compared with unmulched controls (Figure 5B). For wheat, SHS mulching led to a 17% enhancement in the grain yield under normal freshwater irrigation. Under brackish water irrigation, only the dry biomasses of barley plants that

underwent SHS mulching were significantly higher (+44%) than that of barley plants grown in unmulched controls (Figure S13). In 2020, we established an experiment with 450 tomato plants. However, this time, instead of assigning separate plots for specific treatments, we intercalated SHS and unmulched treatments in the same plots. These tomato plants produced a modest 10% increase in the fruit yield compared with that of unmulched controls (Figure S14). We consider that the experimental (intercalated) configuration led to the inadvertent sharing of the enhanced soil moisture beneath the SHS mulch with the neighboring unmulched regions/plants due to capillarity (note: the plants were separated by a distance of approximately 20–40 cm). Nevertheless, the results demonstrated statistical significance ($p = 0.02$) due to greater number of replicates for this crop cycle. Lastly, we investigated the effects of SHS mulching with reduced irrigation (50% of normal irrigation, once a day). Under these conditions, the results were not promising, presumably due to the acute water stress (Figures S11 and 12).

Effects of SHS Mulching on Soil and the Root Microbiome. We identified a total of 6912 bacterial 16S rRNA gene unique SVs associated with root system compartments (root tissues and rhizosphere) and bulk soil samples of barley (6338 SVs) and tomato (6350 SVs; Table S5). Of the tested experimental factors (root system compartments, irrigation type, and SHS mulch overlay), variation (β-diversity) in the ebacterial community was mainly affected by niche compartmentalization of the root system (barley: $R^2 = 0.26$, $F_{2,98} = 18.04$, $p = 0.001$ and tomato: $R^2 = 0.22$, $F_{2,99} = 14.99$, $p = 0.001$; Figure 6A,D), followed by irrigation type, i.e., fresh versus brackish water, (barley: $R^2 = 0.04$, $F_{1,99} = 5.29$, $p = 0.001$
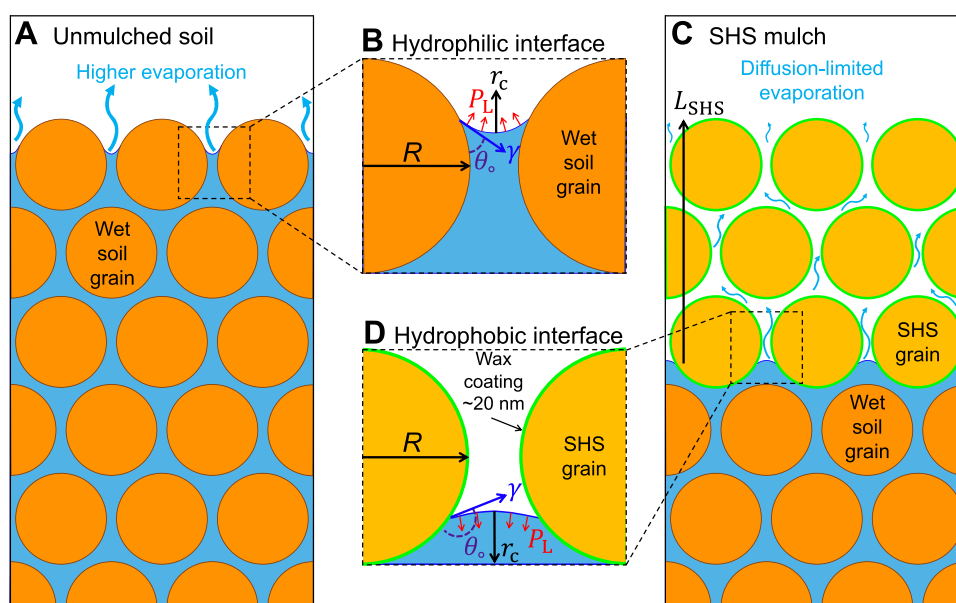
Figure 7. Mechanism for limiting water evaporation from the soil. (A) Water from subsurface irrigation is spontaneously imbibed by the soil media due to (B) positive Laplace pressure, P_L (red arrows). This results in the capillary rise of water, leading to evaporation loss. (C) Water from subsurface irrigation is imbibed by the soil, but this imbibition is arrested at the soil−SHS interface due to (D) negative Laplace pressure. Subsequently, SHS acts as a barrier, limiting diffusion and significantly reducing water loss from the soil.

and tomato: $R^2 = 0.04$, $F_{1,100} = 5.76$, $p = 0.001$; Figure 6B,E). The application of the SHS mulch overlay did not affect the composition of bacterial communities (barley: $R^2 = 0.011$, $F_{1,99} = 1.54$, $p = 0.06$ and tomato: $R^2 = 0.009$, $F_{1,100} = 1.27$, $p = 0.15$; Figure 6C,F). Multiple comparison tests showed that in both crops, the irrigation type induced a significant change in the composition of the bacterial communities associated with different plant root system compartments; in contrast, the SHS mulch overlay had no effect on the composition of the bacterial communities (Table S6). This finding was supported by the number of SVs shared between the treatment with SHS mulches and normal soil, 4954 (78%) for barley and 5024 (79%) for tomato, accounting for 98% of the relative abundance in both crops, (Figure 6G,H). Members of the *Gammaproteobacteria*, *Alphaproteobacteria*, and *Bacteroidetes* followed by *Firmicutes*, *Gemmatimonadetes*, and *Actinobacteria* were the dominant bacterial communities identified (Figure S16).

■ DISCUSSION

The results of the present study underscore the potential of SHS mulching for growing more food and vegetation with limited freshwater resources in arid regions. In this section, we explain the mechanisms and factors underlying the water repellency of SHS and its ability to reduce water loss via evaporation from the topsoil, followed by some arguments for the scalability of this approach.

First, we explain why micron-scale water droplets on individual SHS grains exhibit apparent contact angles of $\theta_o \approx 105°$ (Figure 2E), whereas millimeter-scale water droplets placed on SHS mulches, e.g., a 5 mm-thick layer, exhibit much higher values, i.e., $\theta_A \approx 160°$ (Figure 2A). This dramatic enhancement in water repellency arises from the entrapment of air between the SHS grains as they come into contact with water—a hallmark of superhydrophobicity.[43−48,53] In fact, the apparent macroscale angles can be related to grain-level (actual) angles via the Cassie−Baxter model, $\cos \theta_A = \phi_{LS} \times$ $\cos \theta_o - \phi_{LV}$, where ϕ_{LS} and ϕ_{LV} are the area fractions of the real liquid−solid area and liquid−vapor area normalized by the projected area[54,55] (see ref 56 for the terminology used here). Assuming minimal liquid penetration into the SHS and that the SHS grains are smooth and devoid of reentrant geometries,[52,57] the predicted apparent (macroscopic) contact angle for $\phi_{LS} = 0.1$ and $\phi_{LV} = 0.9$ yields $\theta_{A,P} = 158°$, which is in reasonable agreement with the experimental observation of $\theta_A \approx 160°$. This means that when a water droplet is placed on an SHS mulch, it is practically hovering on air (because only 10% of its area touches the solid).

Next, we explain how SHS governs the fate of water loss via evaporation from the topsoil. First, we emphasize that all the field-scale experiments reported in this study utilized subsurface irrigation. When water comes in contact with common hydrophilic soil particles, the mechanical equilibrium between the interfacial tensions creates a concave meniscus, which drives it in all directions, including upward, due to capillarity (Figure 7A,B). Considering that the particle size of soil ranges from 1 to 1000 μm (Figure 1B), pore sizes between the grains could yield an average radius of curvature of the water meniscus of $r_c \approx 5$ μm. For an actual contact angle of $\theta_o \approx 39°$ for silica, the major component of our soil (please refer to the Supporting Information, Section III, Figure S15), the magnitude of the Laplace or curvature pressure can be determined by the formula $P_L = 2 \gamma_{LV} \times \cos \theta_o \times C_m$, where γ is the surface tension of water, $C_m = 0.5 \times (1/R_1 + 1/R_2)$ is the mean curvature of the liquid−air interface, and R_1 and R_2 are the mutually orthogonal radii of the interfacial curvature. Assuming a spherical symmetry of the air−water interface, $R_1 = R_2 = r_c \approx 5$ μm, which yields $P_L \approx 23$ kPa. This pressure drives the water radially from the subsurface dripping point in all directions, including upward to the topsoil−air interface, where it evaporates (Figures 7A and 2A).

Conversely, when soil moisture rises upward and touches the SHS mulch, the curvature of the air−water interface at the interface of the SHS grains becomes convex (Figure 7C,D).

Therefore, the same Laplace pressure that drives the capillary rise of water prevents its imbibition into the SHS layer, thus keeping it dry (Figure 7D). In fact, the magnitude of this preventive (or negative) Laplace pressure can be calculated using the formula $P_L = 2\ \gamma_{LV} \times \cos\theta_o \times C_m$. We presume that the average value of C_m of the air−water interface in contact with SHS grains of sizes ranging from 100 to 700 μm is $\approx 1/30$ μm^{-1}, which yields $P_L = -1.2$ kPa, a result in reasonable agreement with that of breakthrough pressure experiments. This analysis explains how an SHS layer facilitates a dry porous barrier for water vapor (and other gases).

While liquid water is unable to spontaneously imbibe SHS, water vapor can diffuse through the SHS mulch layer. In fact, the evaporation flux of water from the topsoil and across the SHS mulch can be estimated using Fick's diffusion model $J = -D \times \Delta\varphi / L_{SHS}$, where $\Delta\varphi$ is the gradient in the water vapor concentration across the SHS layer, L_{SHS}, and $D = \frac{\mathcal{D}_w \times \varepsilon \times \delta}{\tau}$ is the effective diffusivity that depends on the diffusivity of water vapor in air, $\mathcal{D}_w$, porosity, ε, constrictivity, δ, and tortuosity, τ, of the granular mulch.[58] Evident from this equation, the thicker the SHS mulch, the lower the evaporation flux, as confirmed in our experiments by the $\sim 1/2 \times$ scaling of the evaporation fluxes with the doubling of the SHS mulch thickness (Figure 3G). SHS also decreases $\Delta\varphi$ by physically covering the topsoil, which reduces its exposure to sunlight and wind.

The capacity of the SHS toward evaporation flux reduction (Figures 3 and 4) is beneficial for enhancing water-use efficiency in plants by channeling the soil moisture conserved under the mulches to transpiration, which enhances photosynthesis.[59] This was supported by our recent pot-scale study in growth chamber experiments, where the SHS mulch enhanced transpiration by 17% under SHS following 78% reduction in evaporation under both normal and reduced irrigation.[60] In the present study, we observed significant yield improvements in the two tomato varieties used and in barley and wheat crops, regardless of the freshwater or brackish water irrigation (Figure 5). By suppressing evaporation, the enhanced soil moisture under SHS mulches likely played a key role in attenuating the effects of salt stress by transporting salts away from the root region via percolation/capillarity, as evidenced by the 39−60% lower sodium concentration in the topsoil ($p < 0.05$, Table S2). Similar effects of mulches in attenuating salt stress have been reported in other studies.[61−63] However, it should be noted that repeated brackish water irrigation would add to cumulative levels of soil salinity.

During the course of the trials, the field station experienced dust storms and daily wind speeds of $\sim 0-15$ ms^{-1} without noticeable loss of SHS or its water-conserving properties.[64] This was due to the relatively larger size and mass of the SHS relative to soil particles (Figure 1B) and due to interparticle friction between SHS grains (Figure S2F). During the later stages of the crop cycle (March−April), soil temperatures in our fields were more than 70 °C. However, this did not compromise the wax coating (bulk melting point $\sim 60-65$ °C); the adhesive force at the sand−wax interface exceeded the weight of the wax, preempting its dripping.[65] Therefore, the integrity of the wax coating was maintained for enhanced soil water conservation under the hot arid field conditions.

In our field trials, we left the SHS mulches in the field after harvesting the crops and observed that the SHS lost its hydrophobicity after about 9−12 months and liquid water can seep in without any resistance. The mixing of the topsoil with the wettable subsoil (by natural factors and/or plowing[66,67]) drives the loss of hydrophobicity due to microbial degradation of paraffin wax.[68] Many soil microorganisms, e.g., *Actinobacteria*, *Proteobacteria*, and *Firmicutes*,[69−71] can degrade a wide range of hydrocarbons.[72,73] As presented in Figures 6 and S16, our rhizosphere environments were mainly dominated by these bacterial groups with wax-degrading potential. By utilizing wax as a source of carbon and energy,[70] these microorganisms are known to remediate water repellency in soils, aiding even water infiltration, seed germination, crop establishment, and higher yields.[74−77] Next, we comment on the effects of paraffin wax on soil. Purified paraffins as those used in our study are easily biodegradable naturally and nontoxic,[78−80] and as "food-grade" compounds, they are commonly utilized in packaging domestic products, including food items.[30−32] These factors render SHS mulches environmentally benign in contrast to plastic mulches, which must be landfilled eventually.[18]

Taken together, the results presented in this study underscore the potential of our bioinspired approach for boosting food production in arid regions. Among its ingredients, paraffin wax is the most inexpensive hydrophobic coating available at an industrial scale, in contrast with costly organic/perfluorinated silanes.[15,81] Furthermore, sand can be directly acquired from the soils. In arid regions, such as the Middle East, soils contain a high percentage of sand in their matrix; for example, the soil in our field station comprised $\sim 80\%$ sand (Figures 1B and S15 and SI Section III). In fact, at present, we are perfecting a solvent-free manufacturing protocol that directly exploits sandy soils and paraffin wax to produce SHS. The resulting SHS also exhibits excellent water repellency (Figure S3).

■ CONCLUSIONS

Through this translational research, we demonstrated how sands or sandy soils, abundant resources in arid regions, can be processed into SHS to produce more food with limited water resources. These benefits are complemented by the low environmental and economic impact of SHS manufacturing and agricultural application. The simplicity of this technology is underscored by the fact that we manufactured over 10 tons of SHS in our laboratory and manually applied it to conduct these field trials (Movie S2). In addition to annual crops, we believe that SHS can be applied to perennial orchards, vineyards, or green zones in cities, such as public parks and green corridors. Arid lands with limited renewable water sources, including parts of South America, Africa, the Middle East, the United States, Australia, China, and India, present vast underused regions with untapped potential to expand their agricultural operations by leveraging this sustainable technology.

■ ASSOCIATED CONTENT

ⓢ Supporting Information

The Supporting Information is available free of charge at https://pubs.acs.org/doi/10.1021/acsagscitech.1c00148.

> Material characterization: ^{13}C NMR, ^{1}H NMR, GCMS, EDS; field trial details: weather conditions, photographs, and biomass and yield data; field soil characterization; and microbial data (PDF)

> Water droplets falling on common sand and superhydrophobic sand (MP4)

> Application of SHS mulches in the tomato field (MP4)

■ AUTHOR INFORMATION

Corresponding Author

Himanshu Mishra − *Water Desalination and Reuse Center (WDRC), Biological and Environmental Science and Engineering (BESE) Division, King Abdullah University of Science and Technology (KAUST), Thuwal 23955-6900, Saudi Arabia;* ⊙ orcid.org/0000-0001-8759-7812; Email: Himanshu.Mishra@kaust.edu.sa

Authors

Adair Gallo, Jr. − *Water Desalination and Reuse Center (WDRC), Biological and Environmental Science and Engineering (BESE) Division, King Abdullah University of Science and Technology (KAUST), Thuwal 23955-6900, Saudi Arabia;* ⊙ orcid.org/0000-0001-5015-8111

Kennedy Odokonyero − *Water Desalination and Reuse Center (WDRC), Biological and Environmental Science and Engineering (BESE) Division, King Abdullah University of Science and Technology (KAUST), Thuwal 23955-6900, Saudi Arabia*

Magdi A. A. Mousa − *Department of Arid Land Agriculture, Faculty of Meteorology, Environment and Arid Land Agriculture, King Abdulaziz University, Jeddah 80208, Saudi Arabia; Department of Vegetables, Faculty of Agriculture, Assiut University, Assiut 71526, Egypt*

Joel Reihmer − *Water Desalination and Reuse Center (WDRC), Biological and Environmental Science and Engineering (BESE) Division, King Abdullah University of Science and Technology (KAUST), Thuwal 23955-6900, Saudi Arabia*

Samir Al-Mashharawi − *Water Desalination and Reuse Center (WDRC), Biological and Environmental Science and Engineering (BESE) Division, King Abdullah University of Science and Technology (KAUST), Thuwal 23955-6900, Saudi Arabia*

Ramona Marasco − *Biological and Environmental Science and Engineering (BESE) Division, King Abdullah University of Science and Technology (KAUST), Thuwal 23955-6900, Saudi Arabia*

Edelberto Manalastas − *Water Desalination and Reuse Center (WDRC), Biological and Environmental Science and Engineering (BESE) Division, King Abdullah University of Science and Technology (KAUST), Thuwal 23955-6900, Saudi Arabia*

Mitchell J. L. Morton − *Biological and Environmental Science and Engineering (BESE) Division, King Abdullah University of Science and Technology (KAUST), Thuwal 23955-6900, Saudi Arabia*

Daniele Daffonchio − *Biological and Environmental Science and Engineering (BESE) Division, King Abdullah University of Science and Technology (KAUST), Thuwal 23955-6900, Saudi Arabia*

Matthew F. McCabe − *Water Desalination and Reuse Center (WDRC), Biological and Environmental Science and Engineering (BESE) Division, King Abdullah University of Science and Technology (KAUST), Thuwal 23955-6900, Saudi Arabia*

Mark Tester − *Biological and Environmental Science and Engineering (BESE) Division, King Abdullah University of Science and Technology (KAUST), Thuwal 23955-6900, Saudi Arabia*

Complete contact information is available at:
https://pubs.acs.org/10.1021/acsagscitech.1c00148

Author Contributions

H.M. conceived the idea of superhydrophobic sand, supervised this research, and coordinated the collaboration. A.G.J. scaled up the SHS manufacturing protocol. M.A.A.M. coordinated daily work in the field and managed crop data collection. JR performed initial feasibility studies with SHS, assisted by M.J.L.M., M.T., and M.A.A.M. A.G.J. and S.M. performed all soil moisture experiments, and MFM advised on sensor calibration and data analysis. M.A.A.M. and M.T. provided expert guidance on field-scale experiments. D.D., R.M., and K.O. performed microbial analysis and analyzed the data. A.G.J. and H.M. analyzed the data from the field-scale experiments. H.M. and A.G.J. wrote the manuscript and the co-authors edited it.

Notes

The authors declare the following competing financial interest(s): Please, note that three of the co-authors, HM, JR, and AGJ have filed a US patent US20200253138A1; other co-authors do not have any competing interests.

The authors declare that all the data supporting the findings of this study are available within the paper and in its Supporting Information.

Raw data have been deposited in the Short Read Archive of the NCBI (Accession numbers: rhizosphere, SUB7136748; root tissue, SUB7211346; and bulk soil, SUB7137862); remaining data are available in the main text and the Supporting Information. The code is available upon request.

■ REFERENCES

(1) Salmon, J. M.; Friedl, M. A.; Frolking, S.; Wisser, D.; Douglas, E. M. Global rain-fed, irrigated, and paddy croplands: A new high resolution map derived from remote sensing, crop inventories and climate data. *Int. J. Appl. Earth Obs. Geoinf.* **2015**, *38*, 321−334.

(2) Shiklomanov, I. A. Appraisal and assessment of world water resources. *Water Int.* **2000**, *25*, 11−32.

(3) Siebert, S.; Burke, J.; Faures, J.-M.; Frenken, K.; Hoogeveen, J.; Döll, P.; Portmann, F. T. Groundwater use for irrigation—a global inventory. *Hydrol. Earth Syst. Sci.* **2010**, *14*, 1863−1880.

(4) HLPE. *Water for Food Security and Nutrition*; High Level Panel of Experts on Food Security and Nutrition of the Committee on World Food Security: Rome, 2015.

(5) Boretti, A.; Rosa, L. Reassessing the projections of the world water development report. *npj Clean Water* **2019**, *2*, No. 15.

(6) Hillel, D. *Introduction to Soil Physics*; Academic Press, 1982.

(7) Gong, D.; Mei, X.; Hao, W.; Wang, H.; Caylor, K. K. Comparison of ET partitioning and crop coefficients between partial plastic mulched and non-mulched maize fields. *Agric. Water Manage.* **2017**, *181*, 23−34.

(8) Rodell, M.; Famiglietti, J. S.; Wiese, D. N.; Reager, J. T.; Beaudoing, H. K.; Landerer, F. W.; Lo, M. H. Emerging trends in global freshwater availability. *Nature* **2018**, *557*, 651−659.

(9) Jury, W. A.; Vaux, H. The role of science in solving the world's emerging water problems. *Proc. Natl. Acad. Sci. U.S.A.* **2005**, *102*, 15715−15720.

(10) Rodell, M.; Velicogna, I.; Famiglietti, J. S. Satellite-based estimates of groundwater depletion in India. *Nature* **2009**, *460*, 999−1002.

(11) Bagla, P. Along the Indus River, Saber Rattling Over Water Security. *Science* **2010**, *328*, No. 1226.

(12) FAO. *The Future of Food and Agriculture—Trends and Challenges*; FAO: Rome, 2017.

(13) Rosa, L.; Chiarelli, D. D.; Rulli, M. C.; Dell'Angelo, J.; D'Odorico, P. Global agricultural economic water scarcity. *Sci. Adv.* **2020**, *6*, No. eaaz6031.

(14) Fears, R.; Canales Holzeis, C.; ter Meulen, V. Designing inter-regional engagement to inform cohesive policy making. *Palgrave Commun.* **2020**, *6*, No. 107.

(15) Salem, M. A.; Al-Zayadneh, W.; Cheruth, A. J. Water conservation and management with hydrophobic encapsulation of sand. *Water Resour. Manage.* **2010**, *24*, 2237−2246.

(16) Guber, A. K.; Smucker, A. J. M.; Berhanu, S.; Miller, J. M. L. Subsurface Water Retention Technology Improves Root Zone Water Storage for Corn Production on Coarse-Textured Soils. *Vadose Zone J.* **2015**, *14*, No. 0166.

(17) Nkurunziza, L.; Chirinda, N.; Lana, M.; Sommer, R.; Karanja, S.; Rao, I.; Romero Sanchez, M. A.; Quintero, M.; Kuyah, S.; Lewu, F.; et al. The potential benefits and trade-offs of using sub-surface water retention technology on coarse-textured soils: Impacts of water and nutrient saving on maize production and soil carbon sequestration. *Front. Sustainable Food Syst.* **2019**, *3*, No. 71.

(18) Kasirajan, S.; Ngouajio, M. Polyethylene and biodegradable mulches for agricultural applications: a review. *Agron. Sustainable Dev.* **2012**, *32*, 501−529.

(19) Zhang, P.; Wei, T.; Cai, T.; Ali, S.; Han, Q.; Ren, X.; Jia, Z. Plastic-film mulching for enhanced water-use efficiency and economic returns from maize fields in semiarid China. *Front. Plant Sci.* **2017**, *8*, No. 512.

(20) Zhang, X.; Yang, L.; Xue, X.; Kamran, M.; Ahmad, I.; Dong, Z.; Liu, T.; Jia, Z.; Zhang, P.; Han, Q. Plastic film mulching stimulates soil wet-dry alternation and stomatal behavior to improve maize yield and resource use efficiency in a semi-arid region. *Field Crops Res.* **2019**, *233*, 101−113.

(21) Eberbach, P.; Humphreys, E.; Kukal, S. The effect of rice straw mulch on evapotranspiration, transpiration and soil evaporation of irrigated wheat in Punjab, India. *Agric. Water Manage.* **2011**, *98*, 1847−1855.

(22) Gross, R. A.; Kalra, B. Biodegradable polymers for the environment. *Science* **2002**, *297*, 803−807.

(23) Mishra, H.; Schrader, A. M.; Lee, D. W.; Gallo, A.; Chen, S. Y.; Kaufman, Y.; Das, S.; Israelachvili, J. N. Time-Dependent Wetting Behavior of PDMS Surfaces with Bioinspired, Hierarchical Structures. *ACS Appl. Mater. Interfaces* **2016**, *8*, 8168−8174.

(24) Shah, F.; Wu, W. Use of Plastic Mulch in Agriculture and Strategies to Mitigate the Associated Environmental Concerns. In *Advances in Agronomy*; Academic Press, 2020; Vol. *164*.

(25) Paluselli, A.; Fauvelle, V.; Galgani, F.; Sempéré, R. Phthalate release from plastic fragments and degradation in seawater. *Environ. Sci. Technol.* **2019**, *53*, 166−175.

(26) Lowry, G. V.; Avellan, A.; Gilbertson, L. M. Opportunities and challenges for nanotechnology in the agri-tech revolution. *Nat. Nanotechnol.* **2019**, *14*, 517−522.

(27) Zhou, L.; Cai, D.; He, L.; Zhong, N.; Yu, M.; Zhang, X.; Wu, Z. Fabrication of a high-performance fertilizer to control the loss of water and nutrient using micro/nano networks. *ACS Sustainable Chem. Eng.* **2015**, *3*, 645−653.

(28) Deng, Y.-q.; White, J. C.; Xing, B.-s. Interactions between engineered nanomaterials and agricultural crops: implications for food safety. *J. Zhejiang Univ., Sci., A* **2014**, *15*, 552−572.

(29) Gilbertson, L. M.; Pourzahedi, L.; Laughton, S.; Gao, X.; Zimmerman, J. B.; Theis, T. L.; Westerhoff, P.; Lowry, G. V. Guiding the design space for nanotechnology to advance sustainable crop production. *Nat. Nanotechnol.* **2020**, *15*, 801−810.

(30) Arunkumar, N.; Banu, G.; Gopalakrishnan, N.; Prakash, A. H. Wax Degrading Bacteria: Scope and Applications in Agriculture. *Int. J. Curr. Microbiol. Appl. Sci.* **2017**, *6*, 649−664.

(31) Zhang, J.; Xue, Q.; Gao, H.; Wang, P. Biodegradation of paraffin wax by crude Aspergillus enzyme preparations for potential use in removing paraffin deposits. *J. Basic Microbiol.* **2015**, *55*, 1326−1335.

(32) Shubik, P.; Saffiotti, U.; Lijinsky, W.; Pietra, G.; Rappaport, H.; Toth, B.; Raha, C. R.; Tomatis, L.; Feldman, R.; Ramahi, H. Studies on the toxicity of petroleum waxes. *Toxicol. Appl. Pharmacol.* **1962**, *4*, 1−62.

(33) ASTM, D. *Standard Test Method for Particle-Size Analysis of Soils (D422-63)*; ASTM International: West Conshohocken, PA, 2007; Vol. *10*.

(34) Brunauer, S.; Emmett, P. H.; Teller, E. Adsorption of gases in multimolecular layers. *J. Am. Chem. Soc.* **1938**, *60*, 309−319.

(35) Seyfried, M. S.; Murdock, M. D. Measurement of soil water content with a 50-MHz soil dielectric sensor. *Soil Sci. Soc. Am. J.* **2004**, *68*, 394−403.

(36) Seyfried, M.; Grant, L.; Du, E.; Humes, K. Dielectric loss and calibration of the Hydra Probe soil water sensor. *Vadose Zone J.* **2005**, *4*, 1070−1079.

(37) Marasco, R.; Rolli, E.; Fusi, M.; Michoud, G.; Daffonchio, D. Grapevine rootstocks shape underground bacterial microbiome and networking but not potential functionality. *Microbiome* **2018**, *6*, No. e01395.

(38) Cherif, H.; Marasco, R.; Rolli, E.; Ferjani, R.; Fusi, M.; Soussi, A.; Mapelli, F.; Blilou, I.; Borin, S.; Boudabous, A. Oasis desert farming selects environment-specific date palm root endophytic communities and cultivable bacteria that promote resistance to drought. *Environ. Microbiol. Rep.* **2015**, *7*, 668−678.

(39) Klindworth, A.; Pruesse, E.; Schweer, T.; Peplies, J.; Quast, C.; Horn, M.; Glöckner, F. O. Evaluation of general 16S ribosomal RNA gene PCR primers for classical and next-generation sequencing-based diversity studies. *Nucleic Acids Res.* **2013**, *41*, No. e1.

(40) Callahan, B. J.; McMurdie, P. J.; Rosen, M. J.; Han, A. W.; Johnson, A. J.; Holmes, S. P. DADA2: High-resolution sample inference from Illumina amplicon data. *Nat. Methods* **2016**, *13*, 581−583.

(41) Anderson, M.; Gorley, R. N.; Clarke, R. K. *Permanova+ for Primer: Guide to Software and Statistical Methods*; Primer-E Limited, 2008.

(42) Oksanen, A.; Blanchet, F.; Friendly, M.; Kindt, R.; Legendre, P.; McGlinn, D.; Wagner, H. *R Package "vegan": Community Ecology Package*, version 2.4-3; R Core Team Vienna, 2017.

(43) Parker, A. R.; Lawrence, C. R. Water capture by a desert beetle. *Nature* **2001**, *414*, 33−34.

(44) Mahadik, G. A.; Hernandez-Sanchez, J. F.; Arunachalam, S.; Gallo, A., Jr.; Cheng, L.; Farinha, A. S.; Thoroddsen, S. T.; Mishra, H.; Duarte, C. M. Superhydrophobicity and size reduction enabled Halobates (Insecta: Heteroptera, Gerridae) to colonize the open ocean. *Sci. Rep.* **2020**, *10*, No. 7785.

(45) Hu, D. L.; Chan, B.; Bush, J. W. The hydrodynamics of water strider locomotion. *Nature* **2003**, *424*, 663−666.

(46) Li, C.; Yu, C.; Zhou, S.; Dong, Z.; Jiang, L. Liquid harvesting and transport on multiscaled curvatures. *Proc. Natl. Acad. Sci. U.S.A.* **2020**, *117*, 23436−23442.

(47) Zheng, Y. M.; Bai, H.; Huang, Z. B.; Tian, X. L.; Nie, F. Q.; Zhao, Y.; Zhai, J.; Jiang, L. Directional water collection on wetted spider silk. *Nature* **2010**, *463*, 640−643.

(48) van Breugel, F.; Dickinson, M. H. Superhydrophobic diving flies (Ephydra hians) and the hypersaline waters of Mono Lake. *Proc. Natl. Acad. Sci. U.S.A.* **2017**, *114*, 13483−13488.

(49) Aussillous, P.; Quéré, D. Liquid marbles. *Nature* **2001**, *411*, 924−927.

(50) Gallo, A.; Tavares, F.; Das, R.; Mishra, H. How particle−particle and liquid−particle interactions govern the fate of evaporating liquid marbles. *Soft Matter* **2021**, *17*, 7628−7644.

(51) Arunachalam, S.; Ahmad, Z.; Das, R.; Mishra, H. Counter-intuitive Wetting Transitions in Doubly Reentrant Cavities as a Function of Surface Make-Up, Hydrostatic Pressure, and Cavity Aspect Ratio. *Adv. Mater. Interfaces* **2020**, *7*, No. 2001268.

(52) Domingues, E. M.; Arunachalam, S.; Nauruzbayeva, J.; Mishra, H. Biomimetic coating-free surfaces for long-term entrapment of air under wetting liquids. *Nat. Commun.* **2018**, *9*, No. 3606.

(53) Das, R.; Ahmad, Z.; Nauruzbayeva, J.; Mishra, H. Biomimetic Coating-free Superomniphobicity. *Sci. Rep.* **2020**, *10*, No. 7934.

(54) Cassie, A. B. D.; Baxter, S. Wettability of porous surfaces. *Trans. Faraday Soc.* **1944**, *40*, 546−550.

(55) Kaufman, Y.; Chen, S.-Y.; Mishra, H.; Schrader, A. M.; Lee, D. W.; Das, S.; Donaldson, S. H.; Israelachvili, J. N. Simple-to-Apply Wetting Model to Predict Thermodynamically Stable and Metastable Contact Angles on Textured/Rough/Patterned Surfaces. *J. Phys. Chem. C* **2017**, *121*, 5642−5656.

(56) Marmur, A.; Della Volpe, C.; Siboni, S.; Amirfazli, A.; Drelich, J. W. Contact angles and wettability: towards common and accurate terminology. *Surf. Innov.* **2017**, *5*, 3−8.

(57) Domingues, E. M.; Arunachalam, S.; Mishra, H. Doubly Reentrant Cavities Prevent Catastrophic Wetting Transitions on Intrinsically Wetting Surfaces. *ACS Appl. Mater. Interfaces* **2017**, *9*, 21532−21538.

(58) Tabor, D. *Gases, Liquids and Solids and Other States of Matter*; Cambridge University Press, 2000.

(59) Kadam, N. N.; Yin, X.; Bindraban, P. S.; Struik, P. C.; Jagadish, K. S. Does morphological and anatomical plasticity during the vegetative stage make wheat more tolerant of water deficit stress than rice? *Plant Physiol.* **2015**, *167*, 1389−1401.

(60) Odokonyero, K.; Gallo, A.; Santos, V. D.; Mishra, H. *Effects of Superhydrophobic Sand Mulching on Evapotranspiration and Phenotypic Responses in Tomatoes (Solanum lycopersicum) under Normal and Reduced Irrigation*; bioRxiv, 2021.

(61) Barbosa, I. J.; Sousa, H. C.; Schneider, F.; Sousa, G. G. d.; Lessa, C. I.; Sanó, L. Mulch with sugarcane bagasse and bamboo straw attenuates salt stress in cowpea cultivation1. *Rev. Bras. Eng. Agric. Ambient.* **2021**, *25*, 485−491.

(62) Canjá, J. F.; Sales, J. R. d. S.; Pinho, L. L.; Sousa, N. I. G.; Lacerda, C. F. d.; Sousa, G. G. d. Production and water use efficiency of peanut under salt stress and soil cover. *Rev. Cienc. Agron.* **2021**, *52*, No. 20210040.

(63) Wang, J.; Liu, H.; Wang, S.; Liu, Y.; Cheng, Z.; Fu, G.; Mo, F.; Xiong, Y. Surface mulching and a sandy soil interlayer suppress upward enrichment of salt ions in salt-contaminated field. *J. Soils Sediments* **2019**, *19*, 116−127.

(64) Johansen, K.; Morton, M. J. L.; Malbeteau, Y. M.; Aragon, B.; Al-Mashharawi, S. K.; Ziliani, M. G.; Angel, Y.; Fiene, G. M.; Negrão, S. S. C.; Mousa, M. A. A.; Tester, M. A.; McCabe, M. F. Unmanned Aerial Vehicle-Based Phenotyping Using Morphometric and Spectral Analysis Can Quantify Responses of Wild Tomato Plants to Salinity Stress. *Front. Plant Sci.* **2019**, *10*, No. 370.

(65) de Gennes, P.-G.; Brodchard-Wyart, F.; Quere, D. *Capillarity and Wetting Phenomena: Drops, Bubbles, Pearls, Waves*; Springer, 2003.

(66) Nadav, I.; Tarchitzky, J.; Chen, Y. Soil cultivation for enhanced wastewater infiltration in soil aquifer treatment (SAT). *J. Hydrol.* **2012**, *470−471*, 75−81.

(67) Davies, S.; Bakker, D.; Scanlan, C.; Gazey, C.; Hall, D.; Riethmuller, G.; Abrecht, D.; Newman, P.; Harding, A.; Hayes, D. In *Deep Soil Cultivation to Create Improved Soil Profiles for Dryland Crop Production*, 2013 Society for Engineering in Agriculture Conference: Innovative Agricultural Technologies for a Sustainable Future; Engineers Australia, 2013; p 410.

(68) Zhang, B.; Yao, S. H.; Hu, F. Microbial biomass dynamics and soil wettability as affected by the intensity and frequency of wetting and drying during straw decomposition. *Eur. J. Soil Sci.* **2007**, *58*, 1482−1492.

(69) Bell, T. H.; Stefani, F. O.; Abram, K.; Champagne, J.; Yergeau, E.; Hijri, M.; St-Arnaud, M. A diverse soil microbiome degrades more crude oil than specialized bacterial assemblages obtained in culture. *Appl. Environ. Microbiol.* **2016**, *82*, 5530−5541.

(70) Okoye, A.; Chikere, C.; Okpokwasili, G. In *Characterization of Potential Paraffin Wax Removing Bacteria for Sustainable Biotechnological Application*, SPE Nigeria Annual International Conference and Exhibition; OnePetro, 2019.

(71) Arunkumar, N.; Gulsar Banu, J.; Gopalakrishnan, N.; Prakash, A. Wax degrading bacteria: Scope and applications in agriculture. *Int. J. Curr. Microbiol. Appl. Sci.* **2017**, *6*, 649−664.

(72) Gutierrez, T. Preparing for the next big oil spill at sea: A microbiological perspective. *J. Mar. Microbiol.* **2018**, *2*, 13−14.

(73) Margesin, R.; Labbe, D.; Schinner, F.; Greer, C.; Whyte, L. Characterization of hydrocarbon-degrading microbial populations in contaminated and pristine alpine soils. *Appl. Environ. Microbiol.* **2003**, *69*, 3085−3092.

(74) Roper, M.; Davies, S.; Blackwell, P.; Hall, D.; Bakker, D.; Jongepier, R.; Ward, P. Management options for water-repellent soils in Australian dryland agriculture. *Soil Res.* **2015**, *53*, 786−806.

(75) Roper, M. M. Potential for remediation of water repellent soils by inoculation with wax-degrading bacteria in south-western Australia. *Biologia* **2006**, *61*, S358−S362.

(76) Abadi Ghadim, A. Water repellency: a whole-farm bio-economic perspective. *J. Hydrol.* **2000**, *231−232*, 396−405.

(77) Hall, D.; Jones, H.; Crabtree, W.; Daniels, T. Claying and deep ripping can increase crop yields and profits on water repellent sands with marginal fertility in southern Western Australia. *Soil Res.* **2010**, *48*, 178−187.

(78) Kumar, P. M.; Anandkumar, R.; Sudarvizhi, D.; Mylsamy, K.; Nithish, M. Experimental and theoretical investigations on thermal conductivity of the paraffin wax using CuO nanoparticles. *Mater. Today: Proc.* **2020**, *22*, 1987−1993.

(79) Suaria, G.; Aliani, S.; Merlino, S.; Abbate, M. The occurrence of paraffin and other petroleum waxes in the marine environment: a review of the current legislative framework and shipping operational practices. *Front. Mar. Sci.* **2018**, *5*, No. 94.

(80) Adlan, N. A.; Sabri, S.; Masomian, M.; Ali, M. S. M.; Rahman, R. N. Microbial biodegradation of paraffin wax in Malaysian crude oil mediated by degradative enzymes. *Front. Microbiol.* **2020**, *11*, No. 2145.

(81) Salem, M. A.; Al-Zayadneh, W.; Schulze, H. F.; Cheruth, A. J. Effect of nano-hydrophobic sand layer on Bermudagrass (Cynodon spp.) in urban landscaping. *Urban Water J.* **2014**, *11*, 167−173.